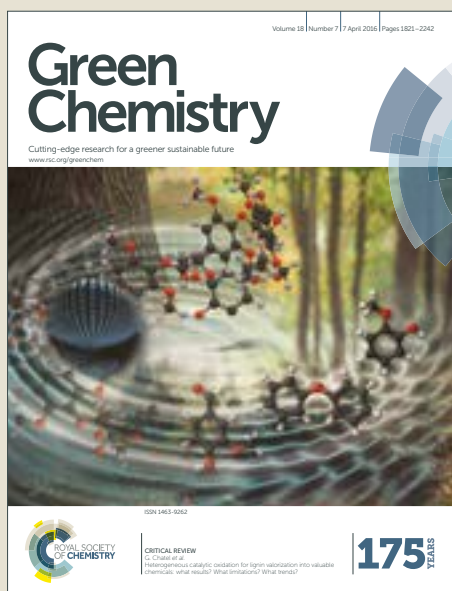


Green Chemistry

Accepted Manuscript



This article can be cited before page numbers have been issued, to do this please use: Y. Fan, S. Cheng, H. Wang, D. Ye, S. Xie, Y. Pei, H. Hu, Z. Li, W. Hua, M. Qiao and B. Zong, *Green Chem.*, 2017, DOI: 10.1039/C7GC00317J.



This is an Accepted Manuscript, which has been through the Royal Society of Chemistry peer review process and has been accepted for publication.

Accepted Manuscripts are published online shortly after acceptance, before technical editing, formatting and proof reading. Using this free service, authors can make their results available to the community, in citable form, before we publish the edited article. We will replace this Accepted Manuscript with the edited and formatted Advance Article as soon as it is available.

You can find more information about Accepted Manuscripts in the [author guidelines](#).

Please note that technical editing may introduce minor changes to the text and/or graphics, which may alter content. The journal's standard [Terms & Conditions](#) and the ethical guidelines, outlined in our [author and reviewer resource centre](#), still apply. In no event shall the Royal Society of Chemistry be held responsible for any errors or omissions in this Accepted Manuscript or any consequences arising from the use of any information it contains.

Nanoparticulate Pt on mesoporous SBA-15 doped with extremely low amount of W as highly selective catalyst for glycerol hydrogenolysis to 1,3-propanediol†

Received 00th January 20xx,
Accepted 00th January 20xx

DOI: 10.1039/x0xx00000x

www.rsc.org/

Yiqiu Fan,^a Shijie Cheng,^a Hao Wang,^a Danhong Ye,^b Songhai Xie,^a Yan Pei,^a Huarong Hu,^b Weiming Hua,^a Zhen Hua Li,^a Minghua Qiao*^a and Baoning Zong*^c

It has been documented that the W-modified Pt catalysts with relatively high tungsten contents are effective for the catalytic transformation of biodiesel-derived glycerol to 1,3-propanediol (1,3-PDO). Herein, we report a new finding that the Pt/W–SBA-15 catalysts with extremely low W/Si atomic ratios ($\leq 1/80$) exhibited excellent catalytic performances in glycerol hydrogenolysis to 1,3-PDO. In particular, the Pt/W–SBA-15 catalyst with the W/Si ratio as low as 1/640 (Pt/W–SBA-15(1/640)) gave rise to the highest 1,3-PDO selectivity of 70.8% at high glycerol conversion of 86.8%, thus rendering the highest 1,3-PDO yield of 61.5%. A combination of the characterization techniques evidenced that tungsten was homogeneously incorporated into SBA-15 in the form of isolated tetragonal WO_4 and of only Lewis acidity. The particle size of Pt evolved in a reversed volcanic curve with the W/Si ratio, with the smallest size being observed on Pt/W–SBA-15(1/640). Control experiments pointed to a strong synergy between the Pt nanoparticles (NPs) and WO_4 in glycerol hydrogenolysis. Probe reaction suggested that Brønsted acid sites were generated *in situ* on the Pt/W–SBA-15 catalysts in the H_2 atmosphere by the reaction between WO_4 and spillover H atoms from the Pt NPs. It is plausible that the hydrided WO_4 functions as the highly selective active centre in the hydrogenolysis of glycerol to 1,3-PDO, while the Pt NPs play the role as the reservoir of spillover H atoms, thus a good matching between the isolated WO_4 and the small-sized Pt NPs is responsible for the superior catalytic performance of Pt/W–SBA-15(1/640).

Introduction

There has been a great surge in the production of biodiesel as an alternative fuel via transesterification of vegetable oils and animal fats to enable the shift of the energy supply from crude oil to biomass. Since producing 100 kg of biodiesel generates simultaneously about 10.5 kg of glycerol,^{1,2} it is of essential importance to improve the value of the redundant glycerol. As one of the higher-value products derived from glycerol, 1,3-PDO serves as a monomer for polytriethylene terephthalate (PTT) that has the softness of nylon, the fluffiness of acrylic fibers, the stain resistance of polyethylene terephthalate (PET), aside from its excellent elasticity and ability to be dyed at room temperature. Unfortunately, the terminal hydroxyl groups of glycerol are more inclined to leave, hence on most catalysts the low-priced 1,2-PDO was produced in greater

amounts,^{3–6} which complies with the result of quantum mechanical calculations that for glycerol the activation energy for the cleavage of the terminal hydroxyl group is 9.6 kJ mol⁻¹ lower than that of the secondary hydroxyl group.⁷ It is apparent that the central challenge in transforming glycerol to 1,3-PDO is the design of catalysts capable of abstracting the secondary hydroxyl group, while leaving the terminal hydroxyl groups in glycerol as well as in 1,3-PDO unaffected.

Up to now, the Pt-sulfated ZrO_2 catalyst,⁸ the Re-modified noble metal catalysts,^{9–11} and the W-modified Pt catalysts^{12–16} are the most prevailing heterogeneous catalysts for glycerol hydrogenolysis to 1,3-PDO. However, the Pt-sulfated ZrO_2 catalyst is only selective in organic medium, which suffers from huge energy consumption to evaporate water from crude glycerol containing ca. 70% of water.¹⁷ The Re-modified noble metal catalysts necessitate sulfuric acid as the additive in most cases,^{9,10,18} which is plagued by corrosiveness to the reactor and unfriendliness to the environment. In addition, Re is far more expensive than W, and the high water solubility of ReO_x undermine the catalytic stability.² Therefore, the W-modified Pt catalysts are more promising for practical applications and become the research focus in recent years.

In a preliminary work, Kurosaka et al. reported that the Pt/ WO_3 / ZrO_2 catalyst with 19.6 wt% of WO_3 could afford the 1,3-PDO selectivity of 24.2% at glycerol conversion of 85.8% in glycerol hydrogenolysis at 443 K using 1,3-dimethyl-2-

^aCollaborative Innovation Centre of Chemistry for Energy Materials, Department of Chemistry and Shanghai Key Laboratory of Molecular Catalysis and Innovative Materials, Fudan University, Shanghai 200433, P. R. China.

E-mail: mhqiao@fudan.edu.cn

^bShanghai Institute of Space Power-Sources, Shanghai 200245, P. R. China.

^cState Key Laboratory of Catalytic Materials and Chemical Engineering, Research Institute of Petroleum Processing, SINOPEC, Beijing 100083, P. R. China.

E-mail: zongbn.ripp@sinopec.com

†Electronic Supplementary Information (ESI) available. See

DOI: 10.1039/x0xx00000x

Table 1 Basic physicochemical properties of the SBA-15, Pt/SBA-15, and Pt/W-SBA-15 samples

Sample	Pt loading ^a (wt%)	W/Si ^a (atomic ratio)	S_{BET}^b ($\text{m}^2 \text{g}^{-1}$)	V_{pore}^b ($\text{cm}^3 \text{g}^{-1}$)	d_{pore}^b (nm)	d_{10}^c (nm)	a^c (nm)	D^d (%)	S_{Pt}^d ($\text{m}^2 \text{g}_{\text{Pt}}^{-1}$)	Particle size (nm) XRD	TEM	Acid amount ^e ($\mu\text{mol}_{\text{NH}_3} \text{g}_{\text{cat}}^{-1}$)
SBA-15	–	–	804	1.3	6.3	10.6	12.2	–	–	–	–	13
Pt/SBA-15	2.91	–	769	1.2	6.4	10.6	12.2	14.0	35	7.3	7.4	41
Pt/W-SBA-15(1/1280)	2.97	1/1271	802	1.4	6.7	10.6	12.3	21.1	52	7.2	6.0	145
Pt/W-SBA-15(1/960)	2.95	1/954	848	1.4	6.8	10.7	12.3	22.0	54	6.1	5.5	151
Pt/W-SBA-15(1/640)	2.96	1/632	926	1.6	6.8	10.7	12.4	23.4	58	6.0	4.7	178
Pt/W-SBA-15(1/320)	2.98	1/316	748	1.3	7.0	10.8	12.4	15.7	39	6.2	7.0	365
Pt/W-SBA-15(1/160)	2.94	1/159	739	1.3	7.0	10.8	12.4	12.8	32	7.1	7.5	422
Pt/W-SBA-15(1/80)	2.97	1/79	708	1.3	7.1	10.8	12.5	10.3	25	9.3	9.2	462

^a Determined by ICP-AES. ^b Determined by N_2 physisorption. ^c Derived from SAXS with $d_{10} = 2\pi/q_{10}$ and $a = d_{10}/\sqrt{3}$. ^d Dispersion and active surface area of Pt determined by CO chemisorption. ^e Determined by NH_3 -TPD.

imidazolidinone as the solvent.¹² Subsequently, Chen and co-workers reported the 1,3-PDO selectivity of 45.6% at glycerol conversion of 70.2% at 403 K over the Pt/ WO_3/ZrO_2 catalyst with 10 wt% of W.¹⁹ Ding and co-workers found that on the Pt/ $\text{WO}_3/\text{TiO}_2/\text{SiO}_2$ catalyst with 5 wt% of WO_3 , the 1,3-PDO selectivity was 50.5% at glycerol conversion of 15.3%.⁴ Zhu et al. prepared the Li-modified Pt- $\text{H}_4\text{SiW}_{12}\text{O}_{40}/\text{ZrO}_2$ catalysts with 20 wt% of $\text{H}_4\text{SiW}_{12}\text{O}_{40}$ and acquired the 1,3-PDO selectivity of 53.6% at glycerol conversion of 43.5%.²⁰ On the SiO_2 -modified Pt/ WO_x/ZrO_2 catalyst with 15 wt% of WO_3 , the 1,3-PDO selectivity was 52.0% at glycerol conversion of 54.3%.²¹ The 1,3-PDO selectivity was improved to 66.1% at glycerol conversion of 64.2% on the Pt- $\text{WO}_x/\text{Al}_2\text{O}_3$ catalyst with 10 wt% of WO_3 .¹⁴ Kaneda and co-workers reported the record-high 1,3-PDO yield of 66–69% over the Pt/ WO_3/AIOOH catalyst with 8.0 wt% of W.¹³ Chary and co-workers developed a Pt- $\text{WO}_3/\text{SBA-15}$ catalyst with 10 wt% of WO_3 being introduced by post-modification of SBA-15, which afforded the 1,3-PDO selectivity of 42% at glycerol conversion of 86%.¹⁵ Recently, Zhang and co-workers reported that the mesoporous WO_x -supported single/pseudo-single atom Pt catalyst showed the 1,3-PDO yield of 21.7% and the highest space-time yield to 1,3-PDO of $3.78 \text{ g g}_{\text{Pt}}^{-1} \text{ h}^{-1}$ among the W-modified Pt catalysts.¹⁶ Without exception, the tungsten contents in all the optimized W-modified Pt catalysts for glycerol hydrogenolysis to 1,3-PDO fall in the range of medium to high surface densities of tungsten according to the classification of Iglesia and co-workers.²² It was generally suggested that the highest Brønsted acidity at relatively high tungsten contents is responsible for the highest selectivity to 1,3-PDO.^{2,4,14,20}

Herein, we report about an unprecedented finding that at extremely low contents of tungsten (W/Si = 0, 1/1280, 1/960, 1/640, 1/320, 1/160, and 1/80, atomic ratio), the Pt/W-SBA-15 catalysts synthesized by incorporating tungsten into SBA-15 via the sol-gel strategy displayed excellent catalytic performances in glycerol hydrogenolysis to 1,3-PDO; details for catalyst preparation, characterization, and catalytic testing can be found in the ESI[†]. The Pt/W-SBA-15 catalyst with the nominal W/Si atomic ratio as low as 1/640, denoted as Pt/W-SBA-15(1/640), performed comparably to the top catalysts reported so far, including the Pt-sulfated ZrO_2 ,⁸ Ir- $\text{ReO}_x/\text{SiO}_2$,⁹

and Pt/ WO_3/AIOOH catalysts.¹³ This is the first work demonstrating and elaborating that tungsten in such a trace amount can impose a dramatic effect on the selectivity to 1,3-PDO in glycerol hydrogenolysis over the W-modified Pt catalyst.

Results and discussion

Composition and texture

By inductively coupled plasma-atomic emission spectroscopy (ICP-AES), we identified that the practical Pt loadings and W/Si ratios on the Pt/SBA-15 and Pt/W-SBA-15 catalysts were close to the nominal loadings (Table 1). Fig. S1[†] shows their N_2 adsorption-desorption isotherms and the corresponding Barrett-Joyner-Halenda (BJH) pore size distribution. The catalysts displayed type IV isotherms with H1 hysteresis loops and the most probable pore size of ca. 6.8 nm, signifying the presence of ordered mesoporous structure. As compiled in Table 1, the Brunauer-Emmett-Teller surface area (S_{BET}) of siliceous SBA-15 was $804 \text{ m}^2 \text{g}^{-1}$, which after the loading of Pt decreased to $769 \text{ m}^2 \text{g}^{-1}$. For the Pt/W-SBA-15 catalysts, the S_{BET} increased with the W/Si ratio first, maximized on Pt/W-SBA-15(1/640), and then decreased monotonically at higher W/Si ratios. CO chemisorption revealed that Pt/W-SBA-15(1/640) displayed the highest active surface area (S_{Pt}) and dispersion (D) of Pt, which decreased upon increasing or decreasing the W/Si ratio (Table 1).

Structure and morphology

The small-angle X-ray scattering (SAXS) patterns of the Pt/SBA-15 and Pt/W-SBA-15 catalysts are presented in Fig. 1. Similar to siliceous SBA-15, they displayed four well-resolved scattering peaks indexible to the (10), (11), (20), and (21) reflections of a two-dimensional hexagonal mesostructure (space group $p6mm$).²³ The (10) reflection shifted slightly to lower q values with the increase in the W/Si ratio, indicating the slight expansion of the interplanar spacing. The d_{10} and unit cell parameter (a) of SBA-15 and W-SBA-15 in the catalysts are summarized in Table 1, both of which increased slightly but monotonically with the W/Si ratio from 0 to 1/80,

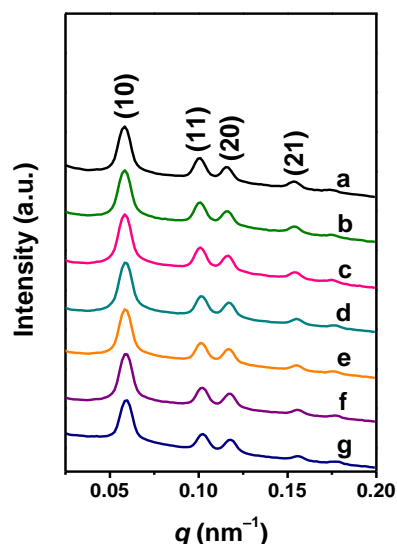


Fig. 1 SAXS patterns of the Pt/W-SBA-15 catalysts with the W/Si atomic ratios of (a) 0, (b) 1/1280, (c) 1/960, (d) 1/640, (e) 1/320, (f) 1/160, and (g) 1/80.

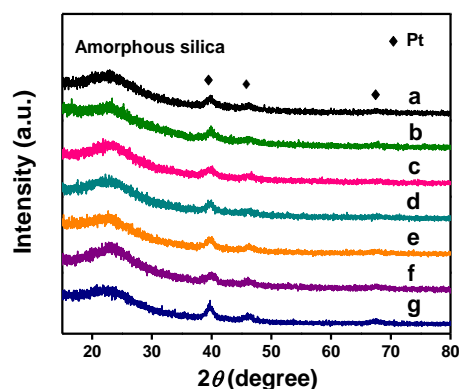


Fig. 2 Wide-angle XRD patterns of the Pt/W-SBA-15 catalysts with the W/Si atomic ratios of (a) 0, (b) 1/1280, (c) 1/960, (d) 1/640, (e) 1/320, (f) 1/160, and (g) 1/80.

signifying the incorporation of tungsten cations (atomic radius 0.68 Å for W^{6+} vs. 0.40 Å for Si^{4+}) into SBA-15.

Fig. 2 shows the wide-angle X-ray diffraction (XRD) patterns of the Pt/SBA-15 and Pt/W-SBA-15 catalysts. Aside from the broad feature at 2θ of ca. 22° from amorphous silica,²⁴ there are small peaks at 2θ of 39.8° , 46.1° , and 67.6° ascribable to the (111), (200), and (220) reflections of the face-centred cubic (fcc) Pt (JCPDS 04-0802), respectively. On the basis of the Scherrer equation and the full width at the half maximum (fwhm) of the (111) peak, the crystallite sizes of Pt were estimated (Table 1). With the increase in the W/Si ratio, the Pt crystallite size decreased gradually from Pt/SBA-15 to Pt/W-SBA-15(1/640), and then increased steadily, which is in agreement with the results of CO chemisorption. On the other hand, there is no diffraction peak assignable to crystalline WO_3 on the Pt/W-SBA-15 catalysts, which is attributed to the extremely low content and high dispersion of tungsten. In line with the XRD results, the Raman spectra of the Pt/W-SBA-15 catalysts as well as the Pt/SBA-15 catalyst were featureless. In contrast, the crystalline monoclinic WO_3 ($m-WO_3$) standard gave distinct Raman bands at 807 (W–O stretching), 714 (W–O

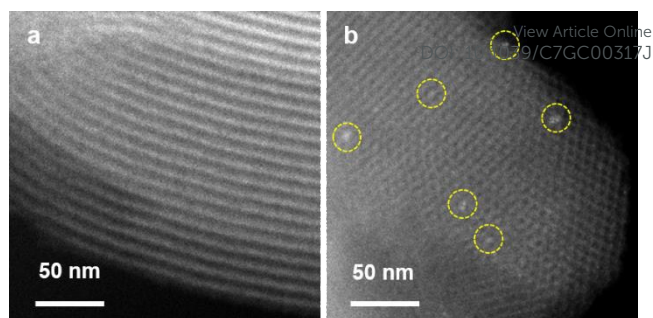


Fig. 3 HAADF-STEM images of (a) the W-SBA-15(1/640) support and (b) the Pt/W-SBA-15(1/640) catalyst.

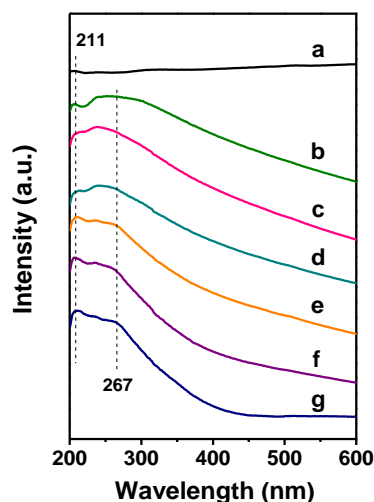


Fig. 4 UV-vis DRS spectra of the Pt/W-SBA-15 catalysts with the W/Si atomic ratios of (a) 0, (b) 1/1280, (c) 1/960, (d) 1/640, (e) 1/320, (f) 1/160, and (g) 1/80.

bending), and 271 cm^{-1} (W–O–W deformation) (Fig. S2†).²⁵

Fig. S3† displays the transmission electron microscopic (TEM) images and particle size distribution (PSD) histograms of the Pt/SBA-15 and Pt/W-SBA-15 catalysts. The mesoporous structure of SBA-15 was well preserved with the doping of tungsten and after the loading of platinum. Analogous to the assignment on Pt/SBA-15, the dark particles on the Pt/W-SBA-15 catalysts are assigned to the Pt NPs instead of the W-containing species. This assignment is further supported by the high-angle annular dark field scanning transmission electron microscopic (HAADF-STEM) images in Fig. 3, which shows no bright dots on the W-SBA-15(1/640) support, while the bright dots are readily visible on Pt/W-SBA-15(1/640). As also compiled in Table 1, with the increase in the W/Si ratio, the size of the Pt NPs decreased first, minimized at 4.7 nm on Pt/W-SBA-15(1/640), and then increased, which is parallel to the evolution of the Pt crystallite size derived from XRD.

Identity of tungsten species

The ultraviolet-visible diffuse reflectance spectroscopic (UV-vis DRS) and Fourier-transform infrared (FTIR) characterizations were carried out to provide insights into the structural details of the tungsten species of extremely low contents and high dispersion. While the UV-vis DRS spectrum

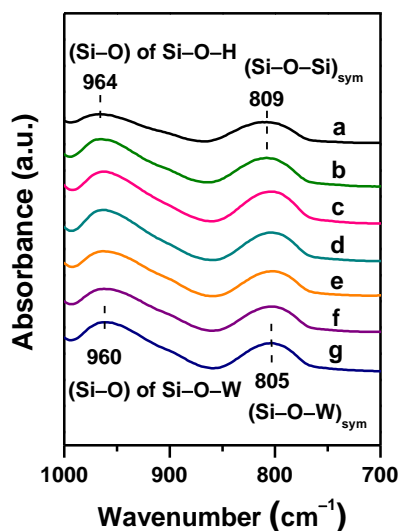


Fig. 5 FTIR spectra of the Pt/W-SBA-15 catalysts with the W/Si atomic ratios of (a) 0, (b) 1/1280, (c) 1/960, (d) 1/640, (e) 1/320, (f) 1/160, and (g) 1/80.

of Pt/SBA-15 is featureless, two bands centred at 211 and 267 nm emerged for the Pt/W-SBA-15 catalysts (Fig. 4). The former is attributed to the isolated tungsten species in a tetrahedral coordination environment (WO_4),^{26,27} whereas the latter can be associated with the tungsten species in a distorted tetrahedral or an octahedral coordination environment,²⁸ which will be further discriminated below.

Fig. 5 shows the FTIR spectra of the Pt/SBA-15 and Pt/W-SBA-15 catalysts. For Pt/SBA-15, the bands at 964 and 809 cm^{-1} are assigned to the Si-O stretching vibration in Si-O-H and the symmetric stretching vibration of Si-O-Si in tetrahedral SiO_4 ,^{29,30} respectively. For the Pt/W-SBA-15 catalysts, with the increase in the W/Si ratio, the maxima of both bands shifted to lower wavenumbers and stabilized at 960 and 805 cm^{-1} . The former is an indication of the incorporation of metal ions into silica with the Si-O stretching vibration being perturbed by neighbouring metal ions.^{31,32} The latter is ascribed to the symmetric stretching vibration of Si-O-W.²⁹ Considering that there is no band at about 875 cm^{-1} characteristic of the W-O stretching vibration of the octahedral WO_6 unit,³³ the UV-vis DRS band at 267 nm in Fig. 4 is then attributed to the tungsten species in a distorted tetrahedral coordination environment. Furthermore, the band characteristic of the asymmetric stretching vibration of W-O-W at about 890 cm^{-1} is also lacking,³⁴ manifesting that the tungsten species are monomeric rather than polymeric. Therefore, the tungsten species on the Pt/W-SBA-15 catalysts with extremely low contents of tungsten can be unambiguously represented as the isolated tetrahedral WO_4 .

Acidic properties

The profiles of the temperature-programmed desorption of NH_3 (NH_3 -TPD) of the Pt/SBA-15 and Pt/W-SBA-15 catalysts are displayed in Fig. S4†. The total acid amounts (n_{NH_3}) determined by integrating the areas under the desorption peaks are also summarized in Table 1. Pt/SBA-15 exhibited a weak desorption feature with low acid amount, which is in

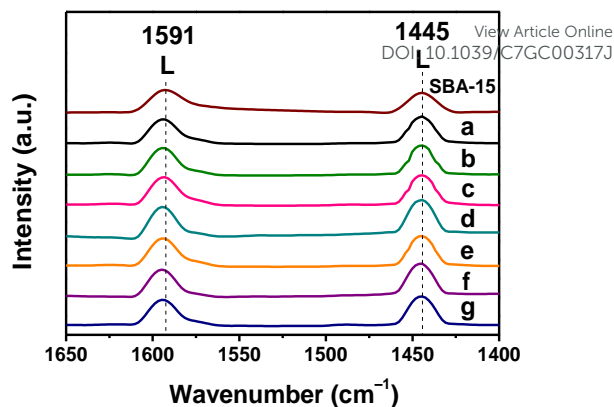


Fig. 6 Py-IR spectra acquired at 373 K on the Pt/W-SBA-15 catalysts with the W/Si atomic ratios of (a) 0, (b) 1/1280, (c) 1/960, (d) 1/640, (e) 1/320, (f) 1/160, and (g) 1/80.

agreement with the poor acidity of siliceous SBA-15.³⁵ The acid amount increased monotonically with the increase in the W/Si ratio, reflecting that the incorporation of tungsten into SBA-15 can generate extra acid sites.³⁶

Fig. 6 presents the pyridine-adsorption FTIR (Py-IR) spectra of the Pt/SBA-15 and Pt/W-SBA-15 catalysts in order to unveil the nature of the acid sites. For siliceous SBA-15, the bands at 1591 and 1445 cm^{-1} are readily ascribable to pyridine coordinated to Lewis acid sites.³⁷ As expected, only bands characteristic of Lewis acid sites were present on Pt/SBA-15. However, even on Pt/W-SBA-15(1/80) with the highest W/Si ratio, tungsten did not invoke Brønsted acid sites that should give band at about 1540 cm^{-1} associated with the W-(OH)-W or W-OH groups.^{38,39} Rather, the amount of Lewis acid sites increased continuously with the W/Si ratio, which can be related to the occurrence of the W=O terminal groups.³⁸

Interaction between Pt and WO_4

Fig. 7 displays the Pt 4f spectra of the Pt/SBA-15 and Pt/W-SBA-15 catalysts; the fitting results are summarized in Table 2. The spectra can be fitted into two groups of doublets with the Pt 4f_{7/2} BEs of ca. 71.1 and 72.8 eV ascribable to Pt^0 and Pt^{2+} , respectively.⁴⁰ As listed in Table 2, the surface $\text{Pt}^{2+}/(\text{Pt}^0 + \text{Pt}^{2+})$ ratio improved from Pt/SBA-15 to Pt/W-SBA-15(1/640), and then descended gradually at higher W/Si ratios. Arribas et al. observed Pt^{2+} on the Pt/ WO_3 - ZrO_2 catalyst and interpreted this species as a sign of the strong interaction between the highly dispersed Pt NPs and surface tungsten species.⁴¹ It is plausible that the Pt^{2+} species are originated from the Pt atoms at the periphery of the Pt NPs that bind to the support by forming the Pt-O-Si/W linkages, which is a well-accepted binding model for metal NPs on oxides.^{42,43} Because the Pt NPs on Pt/W-SBA-15(1/640) are the smallest, this catalyst is anticipated to have the largest number of the peripheral Pt-O-Si/W linkages and hence the highest surface $\text{Pt}^{2+}/(\text{Pt}^0 + \text{Pt}^{2+})$ ratio. This result in turn infers the highest inclination of the W-SBA-15(1/640) support to form the Pt-O-Si/W linkages with the Pt NPs. Consistently, Table 2 also shows that Pt/W-SBA-15(1/640) displayed the highest surface Pt/Si ratio. The XPS results, along with the results of CO chemisorption and TEM, point out that there is an optimal W/Si ratio, namely, 1/640, to

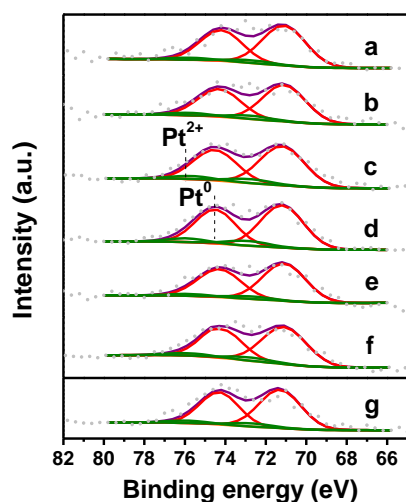


Fig. 7 Pt 4f spectra of the Pt/W-SBA-15 catalysts with the W/Si atomic ratios of (a) 0, (b) 1/1280, (c) 1/960, (d) 1/640, (e) 1/320, (f) 1/160, and (g) 1/80.

Table 2 XPS fitting results of the Pt/SBA-15 and Pt/W-SBA-15 catalysts

Catalyst	Pt 4f _{7/2} BE (eV)		Pt ²⁺ /(Pt ⁰ + Pt ²⁺) ^a	Pt/Si ^a
	Pt ⁰	Pt ²⁺		
Pt/SBA-15	71.1	72.8	0.06	0.51
Pt/W-SBA-15(1/1280)	71.1	72.8	0.08	0.85
Pt/W-SBA-15(1/960)	71.2	72.8	0.09	0.85
Pt/W-SBA-15(1/640)	71.2	72.9	0.10	0.95
Pt/W-SBA-15(1/320)	71.1	72.8	0.08	0.80
Pt/W-SBA-15(1/160)	71.1	72.8	0.08	0.72
Pt/W-SBA-15(1/80)	71.2	72.8	0.07	0.64

^a Atomic ratio.

attain the strongest interaction between Pt and W-SBA-15. On the other hand, because of the extremely low contents of tungsten, the W 4f signals were not discernible even on Pt/W-SBA-15(1/80).

Fig. 8 shows the non-phase corrected radial distribution functions (RDFs) transformed from the Pt L₂-edge $k^3\chi(k)$ data of Pt/SBA-15 and the representative Pt/W-SBA-15(1/1280), Pt/W-SBA-15(1/640), and Pt/W-SBA-15(1/160) catalysts, using Pt foil as the reference. Table 3 summarizes the structural parameters extracted from the extended X-ray absorption fine structure (EXAFS) data. The reliability of the fittings is validated by the close resemblance of the simulated curves to the experimental data (Fig. S5[†]). In Fig. 8, the positions of the main peak of the Pt/SBA-15 and Pt/W-SBA-15 catalysts are identical to that of the first nearest Pt-Pt coordination peak of the Pt foil. However, the much weaker peak amplitudes of the catalysts indicate their much lower Pt-Pt coordination numbers (CNs) as well as much smaller particle sizes.⁴⁴⁻⁴⁶ Moreover, Table 3 shows that the Pt-Pt CN is sensitive to the W/Si ratio. The CN of the Pt-Pt shell decreased

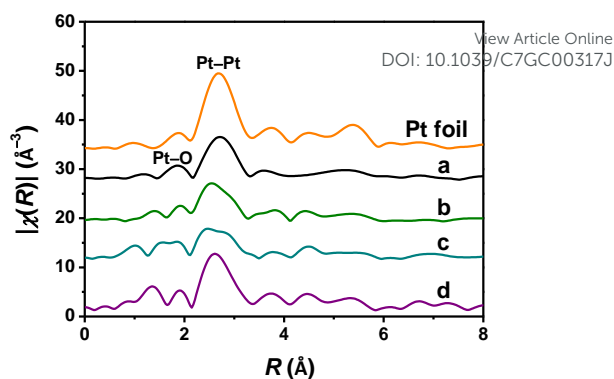


Fig. 8 The RDFs after Fourier transformation of the Pt L₂-edge $k^3\chi(k)$ data of the Pt/W-SBA-15 catalysts with the W/Si atomic ratios of (a) 0, (b) 1/1280, (c) 1/640, and (d) 1/160. The RDF of the Pt foil is included as a reference.

Table 3 Structural parameters derived from the Pt L₂-edge EXAFS data of the Pt foil and the Pt/SBA-15 and Pt/W-SBA-15 catalysts

Sample	Pair	CN ^a	R ^b (Å)	$\Delta\sigma^2$ (10 ⁻³ Å ²)	ΔE_0 (eV)
Pt foil	Pt-Pt	12.0	2.78	5.6	9.3
Pt/SBA-15	Pt-Pt	7.4	2.79	6.1	14.0
	Pt-O	0.3	2.05	8.7	9.3
Pt/W-SBA-15(1/1280)	Pt-Pt	7.4	2.76	6.6	6.8
	Pt-O	0.9	2.00	6.7	9.9
Pt/W-SBA-15(1/640)	Pt-Pt	6.0	2.76	7.2	6.1
	Pt-O	1.1	2.02	1.0	10.4
Pt/W-SBA-15(1/160)	Pt-Pt	10.0	2.77	6.2	11.2
	Pt-O	0.4	2.01	8.1	9.7

^a Error range: $\pm 10\%$. ^b Error range: 0.2 Å.

first, minimized at 4.8 for Pt/W-SBA-15(1/640), and then increased at higher W/Si ratios. The smallest Pt-Pt CN of Pt/W-SBA-15(1/640) is consistent with its smallest Pt NPs. Different from the Pt foil, the Pt/SBA-15 and Pt/W-SBA-15 catalysts had an additional Pt-O coordination shell at ca. 2.03 Å,⁴² which is also present when fitting the k^1 - and k^2 -weighted $\chi(k)$ data. The CN of the Pt-O shell evolved in an inversed trend with respect to that of the Pt-Pt shell, maximizing at 1.1 on Pt/W-SBA-15(1/640). Coupling with its highest surface Pt²⁺/(Pt⁰ + Pt²⁺) ratio, the largest Pt-O CN of Pt/W-SBA-15(1/640) corroborates the assumption that the Pt²⁺ species are associated with the Pt-O-Si/W linkages that aid in anchoring and dispersing small Pt NPs.

Hydrogenolysis of glycerol

The catalytic results of glycerol hydrogenolysis over the Pt/SBA-15 and Pt/W-SBA-15 catalysts at 423 K and 4.0 MPa of H₂ are summarized in Table 4. On Pt/SBA-15, the conversion of glycerol to liquid products (CTL) was only 3.4% after 30 h of reaction, and the primary product was 1-propanol (1-PrOH), followed by 2-PrOH and 1,2-PDO. The selectivity to the target product, 1,3-PDO, was only 8.9%. Upon doping of siliceous SBA-15 with a trace amount of tungsten (W/Si = 1/1280), it is remarkable that the CTL and 1,3-PDO selectivity were boosted respectively by one order of magnitude to 34.5% and more than five folds to 47.5% under the same reaction conditions.

Table 4. The catalytic results of glycerol hydrogenolysis over the Pt/SBA-15 and Pt/W–SBA-15 catalysts^a

Catalyst	Conversion (%)	CTL (%)	Sel. (C% in liquid products)					Yield _{1,3-PDO} (%)	S ₀ ^b (%)	r ₀ ^c	TOF (h ⁻¹)
			1,3-PDO	1,2-PDO	1-PrOH	2-PrOH	Others				
Pt/SBA-15	4.0	3.4	8.9	10.6	63.8	12.9	3.8	0.31	15.8	0.1	2.8
Pt/W–SBA-15(1/1280)	35.6	34.5	47.5	1.8	34.1	7.5	9.1	16.4	52.3	1.1	20.3
Pt/W–SBA-15(1/960)	51.7	50.6	68.3	1.3	22.6	6.8	1.0	34.5	73.4	1.4	25.6
Pt/W–SBA-15(1/640)	88.0	86.8	70.8	1.2	19.8	6.6	1.6	61.5	80.8	4.5	73.6
Pt/W–SBA-15(1/320)	81.9	80.1	64.6	0.8	27.9	6.7	trace	51.8	69.3	4.2	107.3
Pt/W–SBA-15(1/160)	70.1	69.4	52.3	0.9	37.4	5.3	4.1	36.3	60.2	1.7	51.4
Pt/W–SBA-15(1/80)	50.1	49.5	48.4	2.1	42.0	5.2	2.3	24.0	58.6	0.9	34.0

^a Reaction conditions: 200 mg of catalyst, 2.0 g of 30 wt% glycerol aqueous solution, temperature of 423 K, H₂ pressure of 4.0 MPa, stirring rate of 500 rpm, and 30 h. ^b Initial selectivity to 1,3-PDO. ^c Weight-specific activity, unit in mmol g_{cat}⁻¹ min⁻¹. S₀, r₀, and TOF were acquired at CTL of 4.7–8.8%.

The CTL and 1,3-PDO selectivity increased steadily with the W/Si ratio, reached the respective maxima of 86.8% and 70.8% on Pt/W–SBA-15(1/640), thus giving the highest 1,3-PDO yield of 61.5%. Then, the CTL and 1,3-PDO selectivity decreased gradually at higher W/Si ratios. The 1,2-PDO selectivity, on the other hand, was suppressed to no more than 2.1% on all the Pt/W–SBA-15 catalysts, showing that tungsten favourably promotes the abstraction of the secondary hydroxyl group instead of the terminal hydroxyl group of glycerol. On Pt/W–SBA-15(1/640), the initial selectivity to 1,3-PDO (S₀) and the initial weight-specific reaction rate of glycerol (r₀) were 80.8% and 4.5 mmol g_{cat}⁻¹ min⁻¹, respectively, which are also the highest among these catalysts. It is worth noting that the 1,3-PDO yield acquired on Pt/W–SBA-15(1/640) is among the top results reported so far (Table S1[†]), which is only inferior to the 1,3-PDO yield of 66–69% on Pt/WO₃/AlOOH with 8.0 wt% of W at 453 K and 5 MPa of H₂.¹³

Apparently, for the Pt/SBA-15 and Pt/W–SBA-15 catalysts the one with larger S_{Pt}/smaller d_{Pt} gave rise to higher CTL in glycerol hydrogenolysis. Since Pt/W–SBA-15(1/640) had the largest S_{Pt} and the smallest d_{Pt}, it exhibited the highest CTL. However, the CTLs were not directly proportional to S_{Pt} or inversely proportional to d_{Pt}. When we expressed the activity in terms of the turnover frequency (TOF) of glycerol on the basis of r₀ and S_{Pt}, it turns out that the TOFs were closely dependent on the W/Si ratio. In the presence of tungsten, the TOFs were about one order of magnitude of that on Pt/SBA-15 (Table 4), inferring the occurrence of strong synergy between the Pt NPs and the isolated WO₄. It should be noted that the discrepancy in the catalytic performance in the absence and presence of tungsten is not due to the discrepancy in the particle size of Pt. For Pt/SBA-15 and Pt/W–SBA-15(1/160) with similar Pt sizes of 7.4 and 7.5 nm, respectively, they exhibited sharply different activities and selectivities (Table 4).

Tungsten in extremely low amount is very unique in enhancing the activity and selectivity to 1,3-PDO. When tungsten in Pt/W–SBA-15(1/640) was displaced by the same amount of chromium or molybdenum in the same VIB group, or aluminium and vanadium that were frequently adopted to modify SBA-15 in a variety of catalytic applications,^{47–51} the CTLs were only 0.8–7.6%, and the 1,3-PDO selectivities were

only 0.4–2.9% under the same reaction conditions (Table S2[†]).

Tables S3[†] and S4[†] present the influences of the reaction temperature and pressure on the catalytic performance of Pt/W–SBA-15(1/640), respectively. As expected, with the increase of the reaction temperature from 403 K to 443 K, the CTL increased, while the 1,3-PDO selectivity decreased. With the increase of the reaction pressure from 1.0 MPa to 4.0 MPa, both the CTL and 1,3-PDO selectivity increased. Even higher pressure was not attempted for safety concerns. As a result, as far as the 1,3-PDO yield is concerned, the optimum reaction temperature and pressure for Pt/W–SBA-15(1/640) were 423 K and 4.0 MPa, respectively.

As an important character of a catalyst, the reusability of Pt/W–SBA-15(1/640) exhibiting the best catalytic performance was examined. Fig. 9 shows that the CTL decreased insignificantly from the 1st run to the 4th run. The ~2.7% per run CTL drop is more likely caused by material loss due to catalyst attrition in stirred liquid-phase reaction and repetitive catalyst recovery than by the irreversible degradation of the catalyst, which is supported by the essentially invariant product distribution including the selectivity to 1,3-PDO also depicted in Fig. 9. In addition, platinum and tungsten were not detected by ICP–AES in the supernatant after recycling, which excludes the leaching of the active components.

Control experiments

When the W–SBA-15(1/640) support alone was used as the catalyst in glycerol hydrogenolysis under otherwise the same reaction conditions, it gave low CTL of 2.6% and poor 1,3-PDO selectivity of 6.5% (Table S2[†]). Interestingly, physically mixing Pt/SBA-15 with W–SBA-15(1/640) (Pt/SBA-15 + W–SBA-15(1/640)) to attain the same amounts of platinum and tungsten as those in Pt/W–SBA-15(1/640) dramatically improved the CTL to 84.9% (Table S2[†]), which even approaches the CTL on Pt/W–SBA-15(1/640). However, the 1,3-PDO selectivity on the physically mixed catalyst was 36.8%, which is only about one-half of that on Pt/W–SBA-15(1/640) and still lower than those on the Pt/W–SBA-15 catalysts with other W/Si ratios. These results further substantiate the strong synergy between the Pt NPs and the isolated WO₄ on the Pt/W–SBA-15 catalysts, and to a lesser extent, even on the

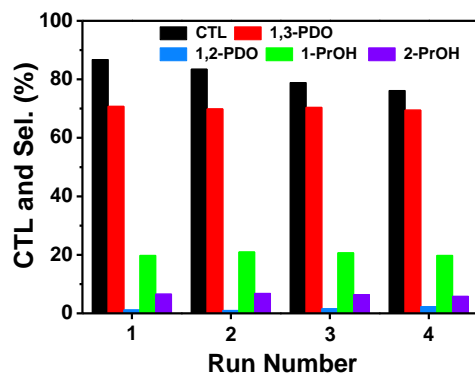


Fig. 9 The CTL and product distribution in glycerol hydrogenolysis over the Pt/W-SBA-15(1/640) catalyst in four successive runs. Reaction conditions: 200 mg of catalyst, 2.0 g of 30 wt% glycerol aqueous solution, temperature of 423 K, H₂ pressure of 4.0 MPa, stirring rate of 500 rpm, and 30 h.

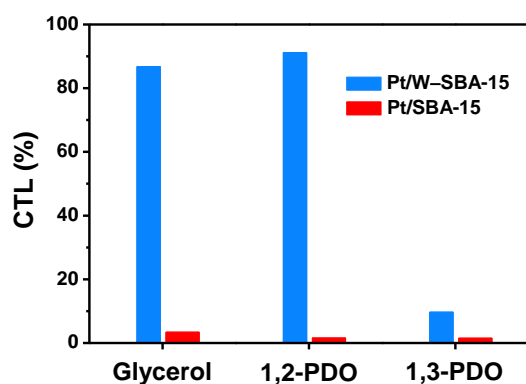
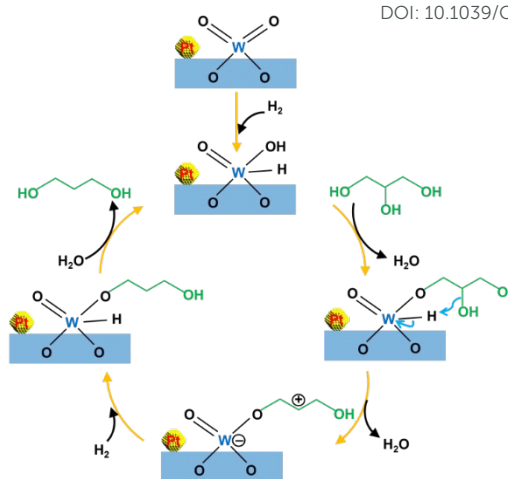


Fig. 10 Hydrogenolysis performance of glycerol, 1,2-PDO, and 1,3-PDO over the Pt/W-SBA-15(1/640) catalyst. Reaction conditions: 200 mg of catalyst, 2.0 g of 30 wt% aqueous solution of the substrate, temperature of 423 K, H₂ pressure of 4.0 MPa, stirring rate of 500 rpm, and 30 h.

physically mixed Pt/SBA-15 + W-SBA-15(1/640) catalyst. Moreover, it turns out that the presence of the Pt NPs and WO₄ on the same catalyst grain is not a necessary prerequisite to a high catalytic activity in glycerol hydrogenolysis, but it is of prime importance to achieve a high 1,3-PDO selectivity.

Further, when we substituted 1,3-PDO for glycerol under otherwise the same reaction conditions on Pt/W-SBA-15(1/640), the CTL of 1,3-PDO was 9.7% (Fig. 10), which is much lower than that of glycerol, showing that the hydrogenolysis of 1,3-PDO is effectively blocked on this catalyst. The poor capability of Pt/W-SBA-15(1/640) to catalyse the hydrogenolysis of 1,3-PDO is advantageous to a high 1,3-PDO selectivity in glycerol hydrogenolysis.

In contrast, when 1,2-PDO was employed as the reactant under otherwise the same reaction conditions on Pt/W-SBA-15(1/640), the CTL of 1,2-PDO amounted to 91.2% (Fig. 10), which is even higher than that of glycerol. This result infers that Pt/W-SBA-15(1/640) is highly capable of catalysing the hydrogenolysis of polyols with both the primary and secondary hydroxyl groups. Moreover, 1-PrOH was the predominant product with high selectivity of 92.9%, while the 2-PrOH selectivity was only 1.0%. The high 1-PrOH to 2-PrOH ratio of



Scheme 1 Proposed reaction mechanism for glycerol hydrogenolysis to 1,3-PDO over the Pt/W-SBA15 catalysts.

92.9 manifests that Pt/W-SBA-15(1/640) is more effective in abstracting the secondary hydroxyl group than the primary hydroxyl group. For comparison, the hydrogenolysis of 1,2-PDO on Pt/SBA-15 resulted in 1-PrOH selectivity of 66.0% and 2-PrOH selectivity of 5.8%. The corresponding 1-PrOH to 2-PrOH ratio was only 11.4. These results unambiguously verify that the presence of the isolated WO₄ preferentially promotes the hydrogenolysis of the secondary hydroxyl group in polyols, thus improving the selectivity to 1,3-PDO in glycerol hydrogenolysis.

Interpretation of the synergy between Pt and W

For the Pt/W-SBA-15 catalysts with the W-SBA-15 supports being synthesized by the sol-gel strategy containing far less amounts of tungsten than those in previous W-modified Pt catalysts for glycerol hydrogenolysis to 1,3-PDO,^{4,12-16,19-21} XRD and Raman indicated that tungsten was highly dispersed without forming crystalline WO₃. UV-vis DRS and FTIR verified that the tungsten species were individually incorporated into SBA-15 through the Si-O-W bonding with tungsten in the tetragonal coordination environment (WO₄). Py-IR revealed that the Pt/W-SBA-15 catalysts contained solely Lewis acid sites. According to Galano et al.,⁵² there are two types of monomeric WO₄, bidentate [(−O−)₂W(=O)₂] and unidentate [(−O−)W(=O)₂(−OH)]. The former only shows Lewis acidity, while the latter shows both Lewis and Brønsted acidity. Therefore, the isolated WO₄ on the Pt/W-SBA-15 catalysts may be more properly depicted as bidentate [(Si-O-)₂W(=O)₂].

The high 1,3-PDO selectivities on the Pt/W-SBA-15 catalysts in glycerol hydrogenolysis with only Lewis acidity seems in contradiction with the overwhelming experience that Brønsted acid sites favour the formation of 1,3-PDO, while Lewis acid sites favour the formation of 1,2-PDO.^{4,8,12,20,53,54} In light of above experimental facts and the reaction mechanisms proposed previously,^{2,9,13,55} we put forward the following

mechanism to account for the unusual catalytic behaviours of the Pt/W–SBA-15 catalysts with extremely low tungsten contents, as illustrated in Scheme 1. With the coexistence of the Pt NPs and the isolated WO_4 , H atoms dissociated from H_2 molecules on the Pt NPs spillover onto WO_4 . The hydrided WO_4 , most likely with one $\text{W}=\text{O}$ group being changed to $\text{H}-\text{W}-\text{OH}$ (Step 1, Scheme 1), plays the role as the active centre for glycerol hydrogenolysis. This assumption is supported by the facts that while the activity of Pt/SBA-15 and W–SBA-15(1/640) alone was poor, when they were mixed together, the activity became comparable to that of Pt/W–SBA-15(1/640). The formation of the hydrided WO_4 represents a physical description of the synergy between the Pt NPs and the isolated WO_4 , and is consistent with the “molecular hydrogen-originated protonic acid site” model proposed on the Pt/ WO_3 – ZrO_2 catalyst in the presence of H_2 .⁵⁶

To validate the *in situ* generation of the protonic acid site, i.e., Brønsted acid site, on the Pt/W–SBA-15 catalysts by spillover H atoms during glycerol hydrogenolysis, we co-fed H_2 with Py when conducting the Py-IR experiment and collected the spectra also in the H_2 atmosphere at 373 K. However, we did not observe the characteristic band of Py on Brønsted acid site at $\sim 1540\text{ cm}^{-1}$ (Fig. S6[†]), possibly due to the low concentration of Brønsted acid sites at ambient H_2 pressure and/or the high reversibility of H atoms migrating between the Pt NPs and tungsten oxide.⁵⁷ Hence, cumene cracking, a sensitive probe reaction catalysed specifically by Brønsted acid sites,⁵⁸ was adopted to examine the Brønsted acidity of Pt/W–SBA-15(1/640). Fig. S7[†] shows that the conversion of cumene using H_2 as the carrier gas was eight folds of that using He as the carrier gas under otherwise the same reaction conditions, which unequivocally confirms that Pt/W–SBA-15(1/640) generates Brønsted acid sites *in situ* in the presence of H_2 .⁴⁰ On the other hand, the possibility of the generation of the Brønsted acidity by hydrolysing the isolated WO_4 with water during the reaction should be minimal, if any, as this would cause the leaching of tungsten and notably deteriorate the catalytic stability, which is not compatible with the good reusability demonstrated above.

After the creation of the active centre, its $\text{W}-\text{OH}$ group acting as Brønsted acid site catalyses the dehydration of the terminal hydroxyl group of glycerol to form 2,3-dihydroxypropoxide (Step 2, Scheme 1) with minimal steric repulsion,⁵⁹ an adsorption configuration also proposed on the Pt/ $\text{WO}_x/\text{Al}_2\text{O}_3$,² Ir– $\text{ReO}_x/\text{SiO}_2$,⁹ Pt– AlO_x/WO_3 ,⁵⁵ and Rh– $\text{ReO}_x/\text{SiO}_2$ catalysts.⁶⁰ Subsequently, the secondary hydroxyl group of 2,3-dihydroxypropoxide attacks the nearby $\text{W}-\text{H}$ bond via a six-membered ring structure. After dehydration, an adsorbed secondary carbocation is formed (Step 3, Scheme 1).^{2,55} Then, two H atoms diffused from the Pt NPs combine with the negatively charged W and the secondary carbocation in a way analogous to the “molecular hydrogen-originated protonic acid site” model.⁵⁶ Namely, one H atom undergoes surface diffusion to secondary carbocation where it releases an electron to the carbocation and becomes a proton, which is stabilized on the negatively charged W. The other H atom combines with the electron trapped at the carbocation and

produces 3-hydroxypropoxide (Step 4, Scheme 1). Finally, the hydrolysis of 3-hydroxypropoxide releases 1,3-PDO and restores the active centre (Step 5, Scheme 1), thus completing the catalytic cycle.

According to Scheme 1, considering that the six-membered ring formed between secondary hydroxyl group and tungsten is more stable than the seven-membered ring formed between terminal hydroxyl group and tungsten, the substrate with the hydroxyl groups at both the primary and secondary positions (glycerol and 1,2-PDO) should be more reactive than 1,3-PDO with only terminal hydroxyl groups, which is validated by the catalytic results illustrated in Fig. 10. Also, the preferential formation of 1,3-PDO and 1-PrOH respectively from glycerol and 1,2-PDO on Pt/W–SBA-15(1/640) (Table 4 and Fig. 10) can be satisfactorily explained by this mechanism. In addition, García-Fernández et al. suggested that the fast hydrogenation of the secondary carbocation is a key step to avoid its further conversion into acrolein, a precursor to 1-PrOH.² Because the surface diffusion of H atoms is usually regarded as a slow step,⁵⁶ it is conceivable that the diffusion distance for H atoms from the Pt NPs to the W-containing carbocation on the Pt/W–SBA-15 catalysts with the Pt NPs and WO_4 on the same catalyst grain is shorter than that on the physically mixed Pt/SBA-15 + W–SBA-15(1/640). Therefore, the hydrogenation of the secondary carbocation is faster and the 1,3-PDO selectivities are higher while the 1-PrOH selectivities are lower on the Pt/W–SBA-15 catalysts than on the physically mixed catalyst (Table S2[†]). Since H_2 dissociation is necessary before becoming H atoms, and the Pt NPs on the Pt/W–SBA-15 catalysts dissociate and store H atoms required for hydrogen spillover, it is anticipated that Pt/W–SBA-15(1/640) with the smallest Pt NPs is the most effective in providing spillover hydrogen to WO_4 considering its largest S_{Pt} available for the dissociation of H_2 (Table 1), thus affording the highest activity and selectivity to 1,3-PDO among the Pt/W–SBA-15 catalysts.

Conclusions

We report for the first time the excellent catalytic performance and the plausible working mechanism of the Pt/W–SBA-15 catalysts with extremely low tungsten contents in the selective production of 1,3-PDO from glycerol. The tungsten species on the Pt/W–SBA-15 catalysts was identified as the isolated WO_4 with Lewis acidity. During the reaction, the synergy between the Pt NPs and WO_4 in the H_2 atmosphere led to the *in situ* generation of the hydrided WO_4 by spillover H atoms from the former to the latter, which functions as the highly selective centre for glycerol hydrogenolysis to 1,3-PDO. The good matching between the dimension of the Pt NPs and the isolated WO_4 is essential to a high 1,3-PDO selectivity. This work affords a new strategy for the design of a high-performance catalyst by deploying extremely low amount of tungsten as the co-catalyst to selectively transforming glycerol to 1,3-PDO.

Acknowledgements

This work was supported by the State Key Research and Development Project of China (2016YFB0301602, 2012CB224804), the National Natural Science Foundation of China (21373055), the Science and Technology Commission of Shanghai Municipality (08DZ2270500), and the Beijing Synchrotron Radiation Facility (BSRF).

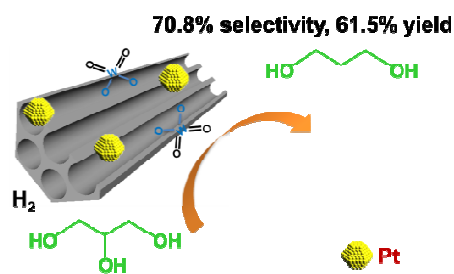
Notes and references

- B. Katryniok, S. Paul, V. Bellière-Baca, P. Rey and F. Dumeignil, *Green Chem.*, 2010, **12**, 2079–2098.
- S. García-Fernández, I. Gandarias, J. Reques, M. B. Güemez, S. Bennici, A. Auroux and P. L. Arias, *J. Catal.*, 2015, **323**, 65–75.
- C. H. Zhou, J. N. Beltramini, Y. X. Fan and G. Q. Lu, *Chem. Soc. Rev.*, 2008, **37**, 527–549.
- L. F. Gong, Y. Lu, Y. J. Ding, R. H. Lin, J. W. Li, W. D. Dong, T. Wang and W. M. Chen, *Appl. Catal. A*, 2010, **390**, 119–126.
- O. M. Daniel, A. DeLaRiva, E. L. Kunkes, A. K. Datye, J. A. Dumesic and R. J. Davis, *ChemCatChem*, 2010, **2**, 1107–1114.
- J. Y. Hu, Y. Q. Fan, Y. Pei, M. H. Qiao, K. N. Fan, X. X. Zhang and B. N. Zong, *ACS Catal.*, 2013, **3**, 2280–2287.
- M. R. Nimlos, S. J. Blanksby, X. Qian, M. E. Himmel and D. K. Johnson, *J. Phys. Chem. A*, 2006, **110**, 6145–6156.
- J. Oh, S. Dash and H. Lee, *Green Chem.*, 2011, **13**, 2004–2007.
- Y. Nakagawa, Y. Shinmi, S. Koso and K. Tomishige, *J. Catal.*, 2010, **272**, 191–194.
- Y. Amada, H. Watanabe, M. Tamura, Y. Nakagawa, K. Okumura and K. Tomishige, *J. Phys. Chem. C*, 2012, **116**, 23503–23514.
- W. T. Luo, Y. Lyu, L. F. Gong, H. Du, T. Wang and Y. J. Ding, *RSC Adv.*, 2016, **6**, 13600–13608.
- T. Kurosaka, H. Maruyama, I. Naribayashi and Y. Sasaki, *Catal. Commun.*, 2008, **9**, 1360–1363.
- R. Arundhathi, T. Mizugaki, T. Mitsudome, K. Jitsukawa and K. Kaneda, *ChemSusChem*, 2013, **6**, 1345–1347.
- S. H. Zhu, X. Q. Gao, Y. L. Zhu and Y. W. Li, *J. Mol. Catal. A*, 2015, **398**, 391–398.
- S. S. Pria, V. P. Kumar, M. L. Kantam, S. K. Bhargava, A. Srikanth and K. V. R. Chary, *Ind. Eng. Chem. Res.*, 2015, **54**, 9104–9115.
- J. Wang, X. C. Zhao, N. Lei, L. Li, L. L. Zhang, S. T. Xu, S. Miao, X. L. Pan, A. Q. Wang and T. Zhang, *ChemSusChem*, 2016, **9**, 784–790.
- S. Kongjao, S. Damronglerd and M. Hunsom, *Korean J. Chem. Eng.*, 2010, **27**, 944–949.
- Amada, Y.; Shinmi, Y.; Koso, S.; Kubota, T.; Nakagawa, Y.; Tomishige, K. *Appl. Catal. B*, 2011, **105**, 117–127.
- L. Z. Qin, M. J. Song and C. L. Chen, *Green Chem.*, 2010, **12**, 1466–1472.
- S. H. Zhu, X. Q. Gao, Y. L. Zhu, Y. F. Zhu, X. M. Xiang, C. X. Hu and Y. W. Li, *Appl. Catal. B*, 2013, **140–141**, 60–67.
- S. H. Zhu, X. Q. Gao, Y. L. Zhu, J. L. Cui, H. Y. Zheng and Y. W. Li, *Appl. Catal. B*, 2014, **158–159**, 391–399.
- D. G. Barton, M. Shtein, R. D. Wilson, S. L. Soled and E. Iglesia, *J. Phys. Chem. B*, 1999, **103**, 630–640.
- D. Y. Zhao, J. L. Feng, Q. S. Huo, N. Melosh, G. H. Fredrickson, B. F. Chmelka and G. D. Stucky, *Science*, 1998, **279**, 548–552.
- J. L. Liu, L. J. Zhu, Y. Pei, J. H. Zhuang, H. Li, H. X. Li, M. H. Qiao and K. N. Fan, *Appl. Catal. A*, 2009, **353**, 282–287.
- L. Salvati, Jr., L. E. Makovsky, J. M. Stencel, F. R. Brown and D. M. Hercules, *J. Phys. Chem.*, 1981, **85**, 3700–3707.
- E. Briot, J. Y. Piquemal, M. Vennat, J. M. Bregeault, G. A. Chottard and J. M. Manoli, *J. Mater. Chem.*, 2000, **10**, 953–958.
- B. Hu, H. Liu, K. Tao, C. R. Xiong and S. H. Zhou, *J. Phys. Chem. C*, 2013, **117**, 26385–26395.
- J. C. Hu, Y. D. Wang and L. F. Chen, *Microporous Mesoporous Mater.*, 2006, **93**, 158–163.
- L. H. Hu, S. F. Ji, Z. Jiang, H. L. Song, P. Y. Wu and Q. Q. Liu, *J. Phys. Chem. C*, 2007, **111**, 15173–15184.
- S. Jambhrunkar, M. H. Yu, J. Yang, J. Zhang, A. Shrotri, L. Endo-Munoz, J. Moreau, G. Q. Lu and C. Z. Yu, *J. Am. Chem. Soc.*, 2013, **135**, 8444–8447.
- X. L. Zhang, C. Y. Yuan, M. Y. Li, B. Gao, X. Y. Wang and X. C. Zheng, *J. Non-Cryst. Solids*, 2009, **355**, 2209–2215.
- P. Wu, T. Tatsumi, T. Komatsu and T. Yashima, *J. Catal.*, 2001, **202**, 245–255.
- S. Rada, M. Rada and E. Culea, *J. Alloys Comp.*, 2013, **552**, 10–13.
- S. Ghosh, S. S. Acharyya, T. Sasaki and R. Bal, *Green Chem.*, 2015, **17**, 1867–1876.
- O. F. Mohammed and E. Vauthey, *J. Phys. Chem. A*, 2008, **112**, 3823–3830.
- X. L. Yang, R. H. Gao, W. L. Dai and K. N. Fan, *J. Phys. Chem. C*, 2008, **112**, 3819–3826.
- I. E. Wachs, *Catal. Today*, 1996, **27**, 437–455.
- A. Massa, M. Andersson, E. Finocchio, G. Busca, F. Lenrick and L. Wallenberg, *J. Catal.*, 2013, **297**, 93–109.
- T. Kitano, T. Hayashi, T. Uesaka, T. Shishido, K. Teramura and T. Tanaka, *ChemCatChem*, 2014, **6**, 2011–2020.
- Y. Y. Nie, S. N. Shang, X. Xu, W. M. Hua, Y. H. Yue and Z. Gao, *Appl. Catal. A*, 2012, **433**, 69–74.
- M. A. Arribas, F. Márquez and A. Martínez, *J. Catal.*, 2000, **190**, 309–319.
- Y. Nagai, T. Hirabayashi, K. Dohmae, N. Takagi, T. Minami, H. Shinjoh and S. Matsumoto, *J. Catal.*, 2006, **242**, 103–109.
- Y. Zhu, L. Tian, Z. Jiang, Y. Pei, S. H. Xie and M. H. Qiao, *J. Catal.*, 2011, **281**, 106–118.
- A. M. Karim, V. Prasad, G. Mpourmpakis, W. W. Lonergan, A. I. Frenkel, J. G. Chen and D. G. Vlachos, *J. Am. Chem. Soc.*, 2009, **131**, 12230–12239.
- P. Bera, K. Priolkar, A. Gayen, P. Sarode, M. Hegde, S. Emura, R. Kumashiro, V. Jayaram and G. Subbanna, *Chem. Mater.*, 2003, **15**, 2049–2060.
- G. B. Zhou, Y. Pei, Z. Jiang, K. N. Fan, M. H. Qiao, B. Sun and B. N. Zong, *J. Catal.*, 2014, **311**, 393–403.
- Z. H. Luan, J. Y. Bae and L. Kevan, *Chem. Mater.*, 2000, **12**, 3202–3207.
- M. Selvaraj and S. Kawi, *Chem. Mater.*, 2007, **19**, 509–519.
- J. Melero, J. Iglesias, J. Arsuaga, J. Sainz-Pardo, P. De Frutos and S. Blazquez, *Appl. Catal. A*, 2007, **331**, 84–94.
- M. Selvaraj and D. Park, *Appl. Catal. A*, 2010, **388**, 22–30.
- F. Schröder, M. Ojeda, N. Erdmann, J. Jacobs, R. Luque, T. Noël, L. Van Meervelt, J. Van der Eycken and E. V. Van der Eycken, *Green Chem.*, 2015, **17**, 3314–3318.
- A. Galano, G. Rodriguez-Gattorno and E. Torres-García, *Phys. Chem. Chem. Phys.*, 2008, **10**, 4181–4188.
- A. Alhanash, E. F. Kozhevnikova and I. V. Kozhevnikov, *Appl. Catal. A*, 2010, **378**, 11–18.
- S. H. Zhu, Y. N. Qiu, Y. L. Zhu, S. L. Hao, H. Y. Zheng and Y. W. Li, *Catal. Today*, 2013, **212**, 120–126.
- T. Mizugaki, T. Yamakawa, R. Arundhathi, T. Mitsudome, K. Jitsukawa and K. Kaneda, *Chem. Lett.*, 2012, **41**, 1720–1722.
- H. Hattori and Y. Ono, *Solid Acid Catalysis-From Fundamentals to Applications*, Pan Stanford Publishing, 2015, pp. 251–253.
- Y. J. Xi, Q. F. Zhang and H. S. Cheng, *J. Phys. Chem. C*, 2014, **118**, 494–501.
- T. Shishido and H. Hattori, *J. Catal.*, 1996, **161**, 194–197.
- V. W. Day, W. G. Klemperer and C. Schwartz, *J. Am. Chem. Soc.*, 1987, **109**, 6030–6044.
- Y. Shinmi, S. Koso, T. Kubota, Y. Nakagawa and K. Tomishige, *Appl. Catal. B*, 2010, **94**, 318–326.

Graphical contents entry

Nanoparticulate Pt on mesoporous SBA-15 doped with extremely low amount of W as highly selective catalyst for glycerol hydrogenolysis to 1,3-propanediol

Yiqiu Fan, Shijie Cheng, Hao Wang, Danhong Ye, Songhai Xie, Yan Pei, Huarong Hu, Weiming Hua, Zhen Hua Li, Minghua Qiao,* and Baoning Zong*



Pt/W-SBA-15 catalyst with extremely low W/Si atomic ratio of 1/640 affords high 1,3-PDO selectivity and yield in glycerol hydrogenolysis.